Article:
Scalisi, J., Ruderman, M.S. and Erdélyi, R. (2023) Generation of vertical flows by torsional Alfvén pulses in zero-beta tubes with a transitional layer. The Astrophysical Journal, 951 (1). 60. ISSN: 0004-637X

https://doi.org/10.3847/1538-4357/acd9ae

The Astrophysical Journal, 951:60 (9pp), 2023 July 1 https://doi.org/10.3847/1538-4357/acd9ae

Generation of Vertical Flows by Torsional Alfvén Pulses in Zero-beta Tubes with a Transitional Layer

Joseph Scalisi[1], Michael S. Ruderman[1,2,3], and Robertus Erdélyi[1,4,5]
[1] Solar Physics and Space Plasma Research Centre, School of Mathematics and Statistics, University of Sheffield, Hicks Building, Hounsfield Road, Sheffield, S3 7RH, UK; robertus@sheffield.ac.uk
[2] Space Research Institute (IKI), Russian Academy of Sciences, Moscow, Russia
[3] Moscow Center for Fundamental and Applied Mathematics, Lomonosov Moscow State University, Moscow, Russia
[4] Department of Astronomy, Eötvös Loránd University, 1/A Pázmány Péter sétány, H-1117, Budapest, Hungary
[5] Gyula Bay Zoltán Solar Observatory (GSO), Hungarian Solar Physics Foundation (HSPF), Petőfi tér 3., Gyula, H-5700, Hungary
Received 2023 March 21; revised 2023 May 10; accepted 2023 May 25; published 2023 July 4

Abstract

Spicule activity in the chromosphere is modeled via the perturbation resulting from the propagation of an Alfvén wave pulse in a magnetic flux tube. Building on previous work, the model is augmented by the inclusion of a finite transitional layer in which the atmospheric density decreases exponentially. This additional complexity of the density stratification provides a more physical representation of the solar atmosphere and improves on the existing model. The wave pulse is introduced at the lower boundary of the flux tube and interacts with the transitional layer, also being partially reflected. The total mass flux induced by the pulse, and the proportion of this pulse that is transmitted through the layer, is calculated and examined in the context of spicules and the solar wind using an example solution. We find that the inclusion of the transitional layer results in more plasma flux being transferred into the upper solar atmosphere when compared with the case of a discontinuity. We examine how varying the parameters of this transitional layer affects the ratio of the flux above and below the layer.

Unified Astronomy Thesaurus concepts: Solar atmosphere (1477); Solar physics (1476); Solar chromosphere (1479); Solar transition region (1532); Solar magnetic fields (1503); Alfven waves (23); Magnetohydrodynamics (1964); Solar magnetic bright points (1984); Theoretical models (2107); Solar spicules (1525); Plasma jets (1263); Jets (870)

1. Introduction

Solar jets and spicules are an important part of the solar and heliospheric system, due to their extreme prevalence on the Sun and their consequently considerable potential to transfer energy and mass—which is relevant to the ongoing investigations of chromospheric and coronal heating and the origin of the mass flux of the solar wind. In order to refine and improve our knowledge of the dynamic features of the solar atmosphere, we must use a variety of methods to consider all components of the system as well as the interactions between different processes. Analytical modeling allows us to consider a simpler version of this complex system—for example, with an initial equilibrium state—and then introduce perturbations or controlled changes in order to examine the effect of specific phenomena, without those features of interest being obscured by other effects. In this paper, we aim to study spicules and model their potential ability to affect the solar wind, by focusing on the effect of torsional Alfvén waves on plasma in a highly magnetic flux tube in a stratified atmosphere.

The local environment of spicules is inhomogeneous because they occur throughout the chromosphere (Sterling 2000; Tsiropoula et al. 2012), where varying local conditions can be expected due to the many dynamic features that dominate the region. Magnetic bright points (MBPs) are an example of relatively compact regions with fields on the order of a kilogauss (Keys et al. 2013) within the photosphere, where they tend to appear in the intergranular lanes (De Wijn et al. 2009). Magnetic forces dominate inside MBPs, and they can be modeled as thin magnetic flux tubes (Cranmer & van Ballegooijen 2005). Torsional Alfvén waves are known to occur in many small-scale solar phenomena including spicules and MBPs (De Pontieu et al. 2012), and the relationship between these features is a subject of ongoing investigation; MBPs have been observed to act as anchor points for spicules, and to exhibit oscillations that are funnelled higher into the atmosphere through spicules (Jess et al. 2012). We have investigated the effects of torsional waves on spicules in our previous works (Scalisi et al. 2021a, 2021b). However, while torsional waves are likely to influence the generation and early evolution of spicules, the vertical stratification of the atmosphere from the footpoints of spicules up to their maximum height (around 5–10 Mm) is also likely to affect their later evolution and decline.

Despite being relatively thin when compared to the extent of the corona or the scale of the solar interior, the chromosphere and transition region form an area of the solar atmosphere over which extreme changes occur, e.g., in density (Makita 2003). Plasma density is generally thought to decrease almost exponentially with height, ranging from the order of 10^{-4}kg m^{-3} at the level of the photosphere (Roberts 2019) up to around 10^{-11}kg m^{-3} in the transition region (Priest 2014). Models of the solar atmosphere as a whole have been able to take this into account (Ferraro & Plumpton 1958; Vernazza et al. 1981); however, more research is needed to determine how this density variation affects the evolution of spicules and their effect on the outer solar atmosphere.

In our recent publications (Scalisi et al. 2021a, 2021b), an analytical model was developed to study the evolution of spicules from their formation to their decline, and to consider the role of torsional Alfvén waves in connection with MBPs and spicules. In this regard, here we continue our efforts to build a model that can take into account the inhomogeneous nature of the chromosphere, i.e., the variation in the properties of the atmospheric plasma that occurs as the height above the photosphere increases. Whereas Scalisi et al. (2021b) involved a discontinuity from which Alfvén waves were reflected, we now include a more realistic continuous density profile that may give significantly different results, which we intend to investigate. Hence, in this article we aim to study how the vertical mass flux resulting from a torsional perturbation is transferred from the chromosphere to the corona, and how this depends on the thickness of a transitional layer. This layer is intended to represent the fact that the most extreme variation of plasma density in the solar atmosphere occurs over a relatively thin region of the upper chromosphere. We are interested in how the stratification of the atmosphere affects the plasma flux into the outer atmosphere, i.e., the difference between the perturbation below and above the transitional layer. In the next section, we describe the equilibrium state and present the governing equations of the model.

2. Model

In this analytical model, beginning with the ideal MHD equations and following on from the method of Scalisi et al. (2021a), we consider a magnetic flux tube that acts as a waveguide for an Alfvén wave pulse. In this context, the vertical background magnetic field is assumed to be strong enough that magnetic forces dominate throughout the tube and thus the plasma beta is much less than unity (Jess et al. 2023). We therefore use the zero-beta approximation and neglect the plasma pressure in comparison with the magnetic forces. The perturbation in the magnetic field generates vertical plasma motion via the ponderomotive Lorentz force.

The structure of the atmosphere is modeled as a three-layered system, with the initial pulse generated in the lower region with constant plasma density, passing through an intermediary transitional layer in which the density decreases exponentially, and finally propagating into another region with low constant density.

2.1. Model Specification

We consider the plasma motion inside a vertical semi-infinite magnetic tube of radius r_0. We use cylindrical coordinates r, θ, z with the z-axis vertical. The equilibrium magnetic field is in the z-direction and has a constant magnitude B_0. We consider the tube boundary to be rigid and disregard the interaction of plasma motion inside the tube with the plasma surrounding it. The tube consists of three regions with different plasma densities inside them. The transitional layer is defined by $L \leqslant z \leqslant L + \ell$, i.e., it begins at some height L above the base of the chromosphere and has a vertical extent or thickness of ℓ. We assume that the density $\rho(z)$ in the transitional layer decreases exponentially, hence the equilibrium plasma density is given by

$$\rho_0(z) = \begin{cases} \rho_1, & 0 \leqslant z \leqslant L, \\ \rho_1 \exp((L - z)/H), & L < z < L + \ell, \\ \rho_2, & z \geqslant L + \ell. \end{cases} \quad (1)$$

Here, H is the scale height in the transitional layer, and ρ_1 and ρ_2 are constants related by $\rho_2 = \rho_1 e^{-\ell/H}$. The plasma motion is described by the ideal magnetohydrodynamic (MHD) equations for cold plasmas:

$$\frac{\partial \boldsymbol{V}}{\partial t} + (\boldsymbol{V} \cdot \nabla)\boldsymbol{V} = \frac{1}{\mu_0 \rho}(\nabla \times \boldsymbol{B}) \times \boldsymbol{B}, \quad (2)$$

$$\frac{\partial \boldsymbol{B}}{\partial t} = \nabla \times (\boldsymbol{V} \times \boldsymbol{B}), \quad (3)$$

where $\boldsymbol{V} = (V_r, V_\theta, V_z)$ is the plasma velocity, $\boldsymbol{B} = (B_r, B_\theta, B_z)$ the magnetic field, ρ the plasma density, and μ_0 the magnetic permeability of free space. The Alfvén speed, v_A, is defined by

$$v_A^2 = \frac{B_0^2}{\mu_0 \rho_0}, \qquad v_A(z) = v_{A1} e^{(z-L)/2H}, \quad (4)$$

where $v_{A1} = v_A(L)$ is the (constant) Alfvén speed below the transitional layer and H is the scale height. It follows that $v_{A2} = v_{A1} e^{\ell/2H}$ is the Alfvén speed above the transitional layer.

Below, we consider the motion with small dimensionless amplitude $\epsilon \ll 1$ and we look for a solution to the problem in the form of expansions

$$\boldsymbol{V} = \epsilon \boldsymbol{V}_1 + \epsilon^2 \boldsymbol{V}_2 + ..., \qquad \boldsymbol{B} = B_0 \boldsymbol{e}_z + \epsilon \boldsymbol{B}_1 + \epsilon^2 \boldsymbol{B}_2 + ..., \quad (5)$$

where $\boldsymbol{e}_z$ is the unit vector in the z-direction. We impose the boundary condition at the tube base

$$B_\theta = \epsilon F(t, r), \quad V_\theta = -\frac{\epsilon v_{A1}}{B_0} F(t, r) \quad \text{at} \quad z = 0, \quad (6)$$

where $F(t, r)$ is a function that defines a localized finite-duration pulse inside the flux tube. This will drive a torsional Alfvén wave propagating upward in the first-order approximation; we will then investigate the effect that this has on the second-order quantities.

2.2. First-order Approximation

In the first-order approximation, we collect the terms of the order of ϵ and then look for the solution of obtained equations in the form of torsional wave. In this wave, only $V_{\theta 1}$ and $B_{\theta 1}$ are nonzero, while other components of the velocity and magnetic field perturbation are zero. The torsional velocity and magnetic perturbations $V_{\theta 1}$ and $B_{\theta 1}$ are therefore related by the first-order equation of motion,

$$\frac{\partial V_{\theta 1}}{\partial t} - \frac{v_A^2}{B_0} \frac{\partial B_{\theta 1}}{\partial z} = 0, \quad (7)$$

as well as the first-order induction equation,

$$\frac{\partial B_{\theta 1}}{\partial t} = \frac{\partial V_{\theta 1}}{\partial z} B_0. \quad (8)$$

Combining Equations (7) and (8), the first-order velocity perturbation is then defined by the equation

$$\frac{\partial^2 V_{\theta 1}}{\partial t^2} - v_A^2(z)\frac{\partial^2 V_{\theta 1}}{\partial z^2} = 0. \tag{9}$$

The solution for the velocity below and above the transitional layer is given by

$$V_{\theta 1} = \begin{cases} V_{\theta 1 i}(t - z/v_{A1}) + V_{\theta 1 r}(t + z/v_{A1}), & z \leqslant L, \\ V_{\theta 1 t}(t - z/v_{A2}), & z \geqslant L + \ell. \end{cases} \tag{10}$$

A similar solution for the magnetic field is

$$B_{\theta 1} = \begin{cases} B_{\theta 1 i}(t - z/v_{A1}) + B_{\theta 1 r}(t + z/v_{A1}), & z \leqslant L, \\ B_{\theta 1 t}(t - z/v_{A2}), & z \geqslant L + \ell. \end{cases} \tag{11}$$

2.2.1. Fourier Transform

To find a solution for Equation (9) in the transitional layer, we introduce the Fourier transform with respect to time,

$$\hat{f}(\omega) = \int_{-\infty}^{\infty} f(t) e^{-i\omega t}\, dt, \quad f(t) = \frac{1}{2\pi}\int_{-\infty}^{\infty} \hat{f}(\omega) e^{i\omega t}\, d\omega. \tag{12}$$

Applying this transform to Equation (9) and using Equation (4) yields

$$\frac{\partial^2 \hat{V}_{\theta 1}}{\partial z^2} + \frac{\omega^2 e^{-(z-L)/H}}{v_{A1}^2}\hat{V}_{\theta 1} = 0. \tag{13}$$

This equation is valid for $L \leqslant z \leqslant L + \ell$. Using the variable substitution,

$$u = \frac{2H\omega}{v_{A1}} \exp\left(-\frac{z - L}{2H}\right), \frac{\partial u}{\partial z} = -\frac{u}{2H}, \frac{\partial^2 u}{\partial z^2} = \frac{u}{4H^2}, \tag{14}$$

so that

$$\frac{\partial \hat{V}_{\theta 1}}{\partial z} = -\frac{u}{2H}\frac{\partial \hat{V}_{\theta 1}}{\partial u}, \quad \frac{\partial^2 \hat{V}_{\theta 1}}{\partial z^2} = \frac{u}{4H^2}\left(u\frac{\partial^2 \hat{V}_{\theta 1}}{\partial u^2} + \frac{\partial \hat{V}_{\theta 1}}{\partial u}\right), \tag{15}$$

then by substituting in (14) and (15), we reduce Equation (13) to the Bessel equation

$$u^2\frac{\partial^2 \hat{V}_{\theta 1}}{\partial u^2} + u\frac{\partial \hat{V}_{\theta 1}}{\partial u} + u^2 \hat{V}_{\theta 1} = 0. \tag{16}$$

The general solution to this equation for $\hat{V}_{\theta 1}$ is

$$\hat{V}_{\theta 1} = C_1(\omega) J_0(u) + C_2(\omega) Y_0(u), \tag{17}$$

where $J_0(u)$ and $Y_0(u)$ are Bessel functions of the first and second type and the zeroth order.

After applying the Fourier transform to the induction Equation (8), we obtain

$$\hat{B}_{\theta 1} = \frac{B_0}{i\omega}\frac{\partial \hat{V}_{\theta 1}}{\partial z} = \frac{iuB_0}{2H\omega}\frac{\partial \hat{V}_{\theta 1}}{\partial u}. \tag{18}$$

Using the relations

$$J_0'(u) = -J_1(u), \quad Y_0'(u) = -Y_1(u), \tag{19}$$

where $J_1(u)$ and $Y_1(u)$ are Bessel functions of the first and second type and the first order, and the prime indicates the derivative, we obtain from Equations (17) and (18):

$$\hat{B}_{\theta 1} = -\frac{iuB_0}{2H\omega}[C_1(\omega) J_1(u) + C_2(\omega) Y_1(u)]. \tag{20}$$

Applying the Fourier transform to Equations (10) and (11), we obtain

$$\hat{V}_{\theta 1} = \begin{cases} e^{-i\omega z/v_{A1}}\hat{V}_{\theta 1 i}(\omega) + e^{i\omega z/v_{A1}}\hat{V}_{\theta 1 r}(\omega), & z \leqslant L, \\ e^{-i\omega z/v_{A2}}\hat{V}_{\theta 1 t}(\omega), & z \geqslant L + \ell. \end{cases} \tag{21}$$

$$\hat{B}_{\theta 1} = \begin{cases} e^{-i\omega z/v_{A1}}\hat{B}_{\theta 1 i}(\omega) + e^{i\omega z/v_{A1}}\hat{B}_{\theta 1 r}(\omega), & z \leqslant L, \\ e^{-i\omega z/v_{A2}}\hat{B}_{\theta 1 t}(\omega), & z \geqslant L + \ell. \end{cases} \tag{22}$$

We note that $\hat{B}_{\theta 1}$ and $\hat{V}_{\theta 1}$ are functions of z that depend on ω and r as parameters.

The magnetic field and velocity must be continuous at the boundaries of the transitional layer. This condition results in

$$\begin{aligned} &e^{-i\omega L/v_{A1}}\hat{V}_{\theta 1 i}(\omega) + e^{i\omega L/v_{A1}}\hat{V}_{\theta 1 r}(\omega) \\ &= C_1(\omega) J_0(u_1) + C_2(\omega) Y_0(u_1), \\ &e^{-i\omega(L+\ell)/v_{A2}}\hat{V}_{\theta 1 t}(\omega) = C_1(\omega) J_0(u_2) + C_2(\omega) Y_0(u_2), \\ &e^{-i\omega L/v_{A1}}\hat{B}_{\theta 1 i}(\omega) + e^{i\omega L/v_{A1}}\hat{B}_{\theta 1 r}(\omega) \\ &= -\frac{iB_0}{v_{A1}}[C_1(\omega) J_1(u_1) + C_2(\omega) Y_1(u_1)], \\ &e^{-i\omega(L+\ell)/v_{A2}}\hat{B}_{\theta 1 t}(\omega) = \frac{-iB_0 e^{-\ell/2H}}{v_{A1}} \\ &\times [C_1(\omega) J_1(u_2) + C_2(\omega) Y_1(u_2)], \end{aligned} \tag{23}$$

where

$$\begin{aligned} u_1 &= u(z = L) = \frac{2H\omega}{v_{A1}}, \\ u_2 &= u(z = L + \ell) = \frac{2H\omega}{v_{A1}} \exp\left(-\frac{\ell}{2H}\right). \end{aligned} \tag{24}$$

We impose the boundary condition

$$B_{\theta 1} = F(t, r) \quad \text{at} \quad z = 0. \tag{25}$$

Using Equation (7) and the definitions of $B_{\theta 1}$ and $V_{\theta 1}$, we obtain the relations

$$V_{\theta 1 i} = -\frac{v_{A1}}{B_0}B_{\theta 1 i}, \quad V_{\theta 1 r} = \frac{v_{A1}}{B_0}B_{\theta 1 r}, \quad V_{\theta 1 t} = -\frac{v_{A2}}{B_0}B_{\theta 1 t}. \tag{26}$$

The same relations are valid for the Fourier transforms of the velocity and magnetic field. Then, we transform the third and fourth equations in Equation (23) to

$$\begin{aligned} &e^{-i\omega L/v_{A1}}\hat{V}_{\theta 1 i}(\omega) - e^{i\omega L/v_{A1}}\hat{V}_{\theta 1 r}(\omega) \\ &= i[C_1(\omega) J_1(u_1) + C_2(\omega) Y_1(u_1)], \end{aligned} \tag{27}$$

$$e^{-i\omega(L+\ell)/v_{A2}}\hat{V}_{\theta 1 t}(\omega) = i[C_1(\omega) J_1(u_2) + C_2(\omega) Y_1(u_2)]. \tag{28}$$

We need to be able to write $V_{\theta 1 t}$ in terms of $V_{\theta 1 i}$ in order to find the mass–flux ratio when we solve the second-order approximation for V_{Z2}. We obtain by adding Equation (27) and the first equation in Equation (23):

$$\begin{aligned} &C_1(\omega)[J_0(u_1) + iJ_1(u_1)] + C_2(\omega)[Y_0(u_1) + iY_1(u_1)] \\ &= 2e^{-i\omega L/v_{A1}}\hat{V}_{\theta 1 i}(\omega). \end{aligned} \tag{29}$$

Subtracting Equation (28) from the second equation in Equation (23), we obtain

$$C_1(\omega)[J_0(u_2) - iJ_1(u_2)] + C_2(\omega)[Y_0(u_2) - iY_1(u_2)] = 0. \tag{30}$$

It follows from Equations (29) and (30) that

$$C_1(\omega) = 2e^{-i\omega L/v_{A1}}\hat{V}_{\theta 1i}(\omega)\frac{(Y_0(u_2) - iY_1(u_2))}{G(\omega)} \tag{31}$$

$$C_2(\omega) = -2e^{-i\omega L/v_{A1}}\hat{V}_{\theta 1i}(\omega)\frac{(J_0(u_2) - iJ_1(u_2))}{G(\omega)}, \tag{32}$$

where

$$G(\omega) = [J_0(u_1) + iJ_1(u_1)][Y_0(u_2) - iY_1(u_2)] - [J_0(u_2) - iJ_1(u_2)][Y_0(u_1) + iY_1(u_1)]. \tag{33}$$

Eliminating C_1 and C_2 from (28) and using the identity

$$J_{\nu+1}(x)Y_\nu(x) - J_\nu(x)Y_{\nu+1}(x) \equiv \frac{2}{\pi x}, \tag{34}$$

yields

$$\hat{V}_{\theta 1t}(\omega) = \frac{2iv_{A2}\hat{V}_{\theta 1i}(\omega)}{\pi\omega HG(\omega)}e^{-i\omega T}, \tag{35}$$

where

$$T = \frac{L}{v_{A1}} - \frac{L+\ell}{v_{A2}}. \tag{36}$$

Equation (35) is then the Fourier-transformed first-order azimuthal velocity perturbation and is the solution to Equation (13). We do not give the expression for $\hat{V}_{\theta 1r}(\omega)$, because it is not used below.

2.2.2. Inverse Fourier Transforms

Now, let us calculate the inverse Fourier transforms. In order to make analytical progress, we first assume that $F(t, r) = 0$ for $t \leqslant 0$ and $t \geqslant \tau$. This means that there is no perturbation before an initial time $t = 0$ and that the driver of the pulse is active only for a finite duration τ, after which there is again no perturbation in the first-order quantities. The leading edge of torsional Alfvén wave driven by the perturbation at $z = 0$ arrives at the lower boundary of the transitional layer at $t = L/v_{A1}$. Before it arrives at this lower boundary, it has the form of a pulse of length τv_{A1}. We assume that this length is much larger than the thickness of the transitional layer and introduce the small parameter $\delta = \ell/\tau v_{A1}$.

The main contribution in $\hat{F}(\omega, r)$, which is the Fourier transform of the function defined in Equation (6), comes from $|\omega|$ smaller than or on the order of $2\pi/\tau$, while $|\hat{F}(\omega, r)| \ll 1$ for $|\omega| \gg 2\pi/\tau$, so that it is enough to consider the Fourier transform only for $|\omega| \lesssim 2\pi/\tau$. Because $\ell/H = 2\ln(v_{A2}/v_{A1})$, we have $H \lesssim \ell$, i.e., the scale height is on the order of, or less than, the thickness of the transitional layer. This enables us to obtain the following estimates:

$$|u_1| = \frac{2H|\omega|}{v_{A1}} \lesssim \frac{4\pi H}{\tau v_{A1}} \lesssim \frac{\ell}{\tau v_{A1}} = \delta \ll 1. \tag{37}$$

Because $|u_2| < |u_1|$, it follows that $|u_2| \lesssim \delta$. Below, in all expressions, we only keep terms on the order of unity, δ, and δ^2, and neglect terms of higher orders with respect to δ. Now, we use the relations (Abramowitz & Stegun 1965, ref. 9.1)

$$\begin{aligned} J_0(x) &= 1 - \frac{x^2}{4} + \mathcal{O}(x^4), \qquad J_1(x) = \frac{x}{2} + \mathcal{O}(x^3), \\ Y_0(x) &= \frac{2}{\pi}\left(\ln\frac{x}{2} + \gamma\right)\left(1 - \frac{x^2}{4}\right) + \frac{x^2}{2\pi} + \mathcal{O}(x^4\ln|x|), \\ Y_1(x) &= -\frac{2}{\pi x} + \frac{x}{\pi}\ln\frac{x}{2} + \frac{x}{2\pi}(2\gamma - 1) + \mathcal{O}(x^3\ln|x|), \end{aligned} \tag{38}$$

where γ is the Euler constant. Using these relations, we obtain

$$G(\omega) \approx \frac{i(v_{A2} + v_{A1})}{\pi H\omega} - \frac{\chi}{\pi}\left[1 + \frac{iH\omega}{v_{A1}}(1 - e^{-\ell/2H})\right], \tag{39}$$

where

$$\chi = \frac{\ell}{H} - \left(\frac{v_{A1}}{v_{A2}} - \frac{v_{A2}}{v_{A1}}\right) = \frac{\ell}{H} + 2\sinh\frac{\ell}{2H} \sim \mathcal{O}(1). \tag{40}$$

Using Equation (39) and the identity

$$\frac{1}{1+x} = 1 - x + x^2 - x^3 + \ldots \tag{41}$$

valid for $|x| \ll 1$, which is the case for

$$x = \frac{i\chi H\omega(1 + iH\omega(1/v_{A1} + 1/v_{A2}))}{v_{A1} + v_{A2}} \lesssim \mathcal{O}(\delta), \tag{42}$$

and taking only the first three terms (up to the order of δ^2), we obtain from Equation (35):

$$\hat{V}_{\theta 1t}(\omega) = \frac{2v_{A2}\hat{V}_{\theta 1i}(\omega)}{v_{A1} + v_{A2}}\left(1 - \frac{i\chi H\omega}{v_{A1} + v_{A2}} - \frac{\chi\ell H\omega^2}{(v_{A1} + v_{A2})^2}\right)e^{-i\omega T}. \tag{43}$$

Now, we can calculate the inverse Fourier transforms:

$$\begin{aligned} V_{\theta 1t}(t) &= \frac{1}{2\pi}\int_{-\infty}^{\infty}\hat{V}_{\theta 1t}(\omega)e^{i\omega t}d\omega \\ &= \frac{v_{A2}}{\pi(v_{A1} + v_{A2})}\int_{-\infty}^{\infty}\left(1 - \frac{i\chi H\omega}{v_{A1} + v_{A2}} - \frac{\chi\ell H\omega^2}{(v_{A1} + v_{A2})^2}\right)\hat{V}_{\theta 1i}(\omega)e^{i\omega(t-T)}d\omega \\ &= \frac{v_{A2}}{\pi(v_{A1} + v_{A2})^2}\left(1 - \frac{\chi H}{v_{A1} + v_{A2}}\frac{\partial}{\partial t} + \frac{\chi\ell H}{(v_{A1} + v_{A2})^2}\frac{\partial^2}{\partial t^2}\right)\int_{-\infty}^{\infty}\hat{V}_{\theta 1i}(\omega)e^{i\omega(t-T)}d\omega \\ &= \frac{2v_{A2}}{v_{A1} + v_{A2}}\left[V_{\theta 1i}(t - T) - \frac{\chi HV'_{\theta 1i}(t - T)}{v_{A1} + v_{A2}} + \frac{\chi\ell HV''_{\theta 1i}(t - T)}{(v_{A1} + v_{A2})^2}\right], \end{aligned} \tag{44}$$

where the prime indicates the derivative. Thus, we have an approximate solution for the first-order Equation (9).

2.3. Second-order Approximation

Now, we consider the second-order quantities in the MHD equations, which depend on the solutions we have found for the first-order quantities. This will introduce a vertical perturbation of the plasma due to the ponderomotive Lorentz force.

In the second-order approximation, we collect the terms on the order of ϵ^2 in the z-component in Equation (2). This yields

$$\frac{\partial V_{Z2}}{\partial t} = -\frac{1}{2\mu_0\rho_0(z)}\frac{\partial}{\partial z}(B_{\theta 1}^2). \tag{45}$$

The torsional Alfvén wave arrives at the transitional layer at $t = L/v_{A1}$. Before that time, there is no reflected wave in the region $z < L$, i.e., $V_{\theta 1} = V_{\theta 1i}$. Hence, for $t < L/v_{A1}$ we obtain using Equations (8), (26), and (45) that, below the transitional layer,

$$\frac{\partial V_{Z2i}}{\partial t} = \frac{1}{2v_{A1}}\frac{\partial}{\partial t}(V_{\theta 1i}^2). \tag{46}$$

Because there are no perturbations for $t \leqslant 0$, it follows from this equation that for $t < L/v_{A1}$ there is only the initial wave, so

$$V_{Z2i} = \frac{1}{2v_{A1}}V_{\theta 1i}^2(t - z/v_{A2}). \tag{47}$$

In the region above the transitional layer, there is only transmitted wave, as defined in Equation (10). So, again using Equations (8), (26), and (45) but considering the region $z > L + \ell$, we have

$$\frac{\partial V_{Z2t}}{\partial t} = \frac{1}{2v_{A2}}\frac{\partial}{\partial t}(V_{\theta 1t}^2). \tag{48}$$

Because there are no perturbations for $t \leqslant 0$, we obtain from Equation (48) using Equation (44):

$$\begin{aligned} V_{Z2t} &= \frac{2v_{A2}}{(v_{A1}+v_{A2})^2} \\ &\times \left[V_{\theta 1i}(\Theta) - \frac{\chi H V'_{\theta 1i}(\Theta)}{v_{A1}+v_{A2}} + \frac{\chi \ell H V''_{\theta 1i}(\Theta)}{(v_{A1}+v_{A2})^2}\right]^2 \\ &\approx \frac{2v_{A2}}{(v_{A1}+v_{A2})^2}\left\{V_{\theta 1i}^2(\Theta) - \frac{2\chi H}{v_{A1}+v_{A2}}V_{\theta 1i}(\Theta)V'_{\theta 1i}(\Theta)\right. \\ &\left. + \frac{\chi H}{(v_{A1}+v_{A2})^2}[\chi H(V'_{\theta 1i}(\Theta))^2 + 2\ell V_{\theta 1i}(\Theta)V''_{\theta 1i}(\Theta)]\right\}. \end{aligned} \tag{49}$$

Here, $\Theta = t - T - z/v_{A2}$. Now, we calculate the total mass flux through the tube cross section below and above the transitional layer. We assume that the function $F(t, r)$ is factorized and can be written as $F(t, r) = \Phi(t)\Psi(r)$. It is convenient to calculate the incoming mass flux at $z = 0$, which is then given by

$$M_i = 2\pi\rho_1\int_0^{r_0} r\,dr\int_0^{\tau} V_{Z2i}(t)dt, \tag{50}$$

where r_0 is the tube radius. Using Equations (6) and (47), we transform this expression to

$$M_i = \frac{\pi\epsilon^2\rho_1 v_{A1}}{B_0^2}\int_0^{r_0}\Psi^2(r)r\,dr\int_0^{\tau}\Phi^2(t)dt. \tag{51}$$

The total mass flux through any tube cross section above the transitional layer is the same at any $z > L + \ell$. It follows from Equation (49) that V_{Z2t} is different from zero only for $0 < \Theta < \tau$, **that is for $T + z/v_{A2} < t < \tau + T + z/v_{A2}$. Hence,

$$M_t = 2\pi\rho_2\int_0^{r_0} r\,dr\int_{T+z/v_{A2}}^{\tau+T+z/v_{A2}} V_{Z2t}(t)dt. \tag{52}$$

Although z is present in this expression, the result will be the same for any $z > L + \ell$. Using Equation (49) and the integration variable substitution, we obtain

$$\begin{aligned} I &\equiv \int_{T+z/v_{A2}}^{\tau+T+z/v_{A2}} V_{Z2t}(t)dt \\ &= \frac{2v_{A2}}{(v_{A1}+v_{A2})^2}\int_0^{\tau}\left\{V_{\theta 1i}^2(\Theta) - \frac{2\chi H}{v_{A1}+v_{A2}}V_{\theta 1i}(\Theta)V'_{\theta 1i}(\Theta)\right. \\ &\left. + \frac{\chi H}{(v_{A1}+v_{A2})^2}[\chi H(V'_{\theta 1i}(\Theta))^2 + 2\ell V_{\theta 1i}(\Theta)V''_{\theta 1i}(\Theta)]\right\}d\Theta. \end{aligned} \tag{53}$$

Using integration by parts and Equation (40), we transform this expression to

$$\begin{aligned} I = \frac{2v_{A2}}{(v_{A1}+v_{A2})^2}\int_0^{\tau}\left(V_{\theta 1i}^2(\Theta) + \left[H^2\left(\frac{1}{v_{A1}} - \frac{1}{v_{A2}}\right)^2\right.\right. \\ \left.\left. - \frac{\ell^2}{(v_{A1}+v_{A2})^2}\right](V'_{\theta 1i}(\Theta))^2\right)d\Theta. \end{aligned} \tag{54}$$

Substituting this expression in Equation (52) and using Equation (6) yields

$$\begin{aligned} M_t = \frac{4\epsilon^2\pi\rho_2 v_{A2}v_{A1}^2}{B_0^2(v_{A1}+v_{A2})^2}\int_0^{r_0}\Psi^2(r)r\,dr\left(\int_0^{\tau}\Phi^2(t)dt\right. \\ \left. + \left[H^2\left(\frac{1}{v_{A1}} - \frac{1}{v_{A2}}\right)^2 - \frac{\ell^2}{(v_{A1}+v_{A2})^2}\right]\int_0^{\tau}(\Phi'(t))^2\,dt\right), \end{aligned} \tag{55}$$

where we changed the integration variable from Θ to t. We note that H is proportional to ℓ such that $\ell/H = 2\ln(\alpha)$ is fixed when v_{A1} and v_{A2} are given, where $\alpha = v_{A2}/v_{A1}$. Thus, we see that the term proportional to the thickness of the transitional layer squared (ℓ^2, or equivalently H^2) in the square brackets in Equation (55) gives the correction to M_t related to the substitution of the discontinuity by the smooth transitional layer, and because $\alpha > 1$, it follows that this correction is always positive. We recover the total mass flux due to the transmitted wave in the case of a discontinuity by taking $\ell = 0$ (or equivalently $H = 0$).

To give an example, we take

$$\Phi(t) = A\left(1 - \cos\frac{2\pi t}{\tau}\right), \qquad 0 < t < \tau, \tag{56}$$

where A is a constant and $\Phi(t)$ is otherwise zero. This represents the driver of the wave, which is active for a finite duration τ, creating a wave pulse. Then we obtain

$$\int_0^{\tau}\Phi^2(t)dt = \frac{3\tau A^2}{2}, \qquad \int_0^{\tau}(\Phi'(t))^2\,dt = \frac{2\pi^2A^2}{\tau}. \tag{57}$$

Using these results, we find that the ratio of the second term in the square brackets in Equation (55) to the first one is

$$\begin{aligned} \lambda &= \frac{4\pi^2}{3\tau^2}\left[H^2\left(\frac{1}{v_{A1}} - \frac{1}{v_{A2}}\right)^2 - \frac{\ell^2}{(v_{A1}+v_{A2})^2}\right] \\ &= \frac{4\pi^2}{3}\left(\frac{\ell}{v_{A1}\tau}\right)^2\left[\left(\frac{1-\alpha}{2\alpha\ln(\alpha)}\right)^2 - \frac{1}{(1+\alpha)^2}\right]. \end{aligned} \tag{58}$$

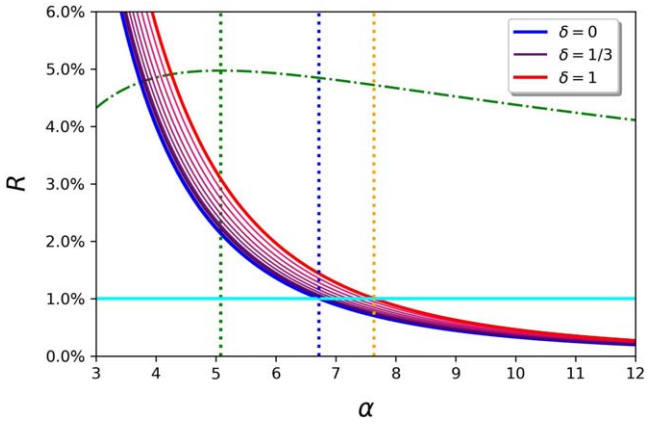

Figure 1. A plot of the mass–flux ratio R against α, showing the effect of varying δ and thus the thickness of the transitional layer. Here, we consider multiple values of δ in the range $0 < \delta < 1$. It should be noted that $\delta = 1$ is included as an extreme case for the sake of comparison, but the model requires a thin layer, i.e., $\delta \ll 1$. The one percent transmission threshold is shown as a cyan line that intersects with the $\delta = 0$ curve of the ratio at $\alpha = 6.717$ (blue dotted line) and with the $\delta = 1$ curve of the ratio at $\alpha = 7.638$ (orange dotted line). Also shown is the proportion of transmitted mass that is due to the effect of the transitional layer, λ (green dotted–dashed curve) for $\delta = 1/3$, with the maximum indicated at $\alpha = 5.082$ (green dotted line).

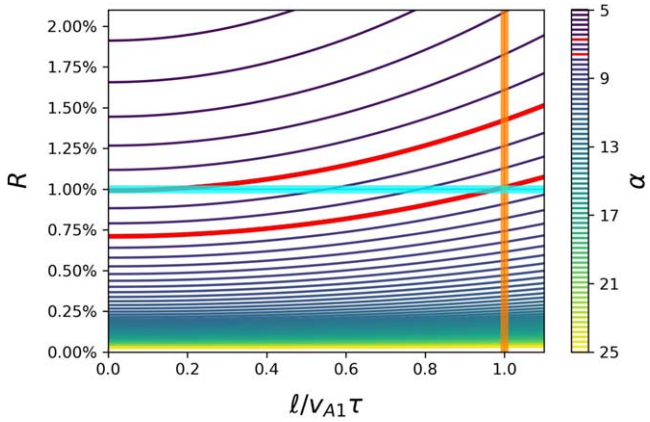

Figure 2. Plots of the mass–flux ratio R against the thickness of the transitional layer $\ell/v_{A1}\tau$ (scaled by the length of the pulse), illustrating the effect of varying α. Here, we consider multiple values of α in the range $5 < \alpha < 25$. The 1% transmission threshold is shown as a cyan line, and the line $\ell = v_{A1}\tau$ as an orange line (we note that $\ell > v_{A1}\tau$ is beyond the scope of the model). Highlighted in red are the values of $\alpha = 6.717$ and $\alpha = 7.638$.

This ratio represents the proportion of the transmitted mass that is due to the effect of the transitional layer, compared to the case of the discontinuity. It is maximized at around $\alpha = 5.082$, when it is approximately equal to $0.447(\ell/\tau v_{A1})^2 = 0.447\delta^2$. Because we have $\delta \ll 1$, the additional transmitted mass due to the effect of the transitional layer must be much less than 44.7% of the total transmitted mass, for any feasible value of α. If, in addition, we take $\delta = 1/3$ as an example satisfying the thin-layer requirement, then we obtain that the ratio of two terms is 0.0497. Hence, in this case, the transmitted flux is greater by approximately 5% than in the case of discontinuity (illustrated in Figure 1). This is encouraging because it suggests that the actual density-stratified solar atmosphere would most likely allow for some spicular material to pass through the chromosphere as a result of torsional Alfvén waves.

We can also find the ratio R of the relative mass flux, i.e., the ratio of the mass of plasma that moves due to the transmitted wave through a given surface $z > L + \ell$ above the transitional layer, as a proportion of the plasma that moves due to the initial wave through a surface $z < L$:

$$R = \frac{M_t}{M_i} = \frac{4}{\alpha(1+\alpha)^2} \times \left(1 + \frac{4\pi^2}{3}\left(\frac{\ell}{v_{A1}\tau}\right)^2\left[\left(\frac{1-\alpha}{2\alpha\ln(\alpha)}\right)^2 - \frac{1}{(1+\alpha)^2}\right]\right). \quad (59)$$

Notably, this is similar to the mass–flux ratio found in Scalisi et al. (2021b) (Equation (32) in that paper) but with an extra term proportional to ℓ^2, hence it is clear that the inclusion of the transitional layer has had a quantifiable effect on the model. The ratio R is shown in Figure 1. We now explore how the mass–flux ratio changes due to the extra term introduced as a result of considering a transitional layer sandwiched between the chromosphere and the low corona, in the next section.

3. Discussion

The result from this model depends on how we specify v_{A1}, τ, H, and α. However, we are particularly interested in how the ratio changes depending on the thickness of the transitional layer ℓ while the other variables remain constant (although we can consider various discrete cases). Therefore, we will have different values for the scale height $H = l/2\ln(\alpha)$ when we vary ℓ, while considering a particular value of α. Because we will consider various cases, it may be helpful to explore physical constraints for the values of our parameters.

In strongly magnetic regions of the lower solar atmosphere inside a flux tube, the Alfvén speed would be on the order of 10 km s^{-1}, with some estimates suggesting values between 7.7 km s^{-1} (Roberts 2019) and 22 km s^{-1} (Jess et al. 2009). Taking the latter value and using Equation (4), this corresponds to an estimate for the density ρ_1 in the lower layer of the model of around 1.64×10^{-8} g cm^{-3}, with a kilogauss-strength background magnetic field. Higher in the atmosphere, the Alfvén speed increases by at least an order of magnitude (Vernazza et al. 1973), with estimates of 1000 km s^{-1} or more in the corona (Tomczyk et al. 2007; van Ballegooijen et al. 2011). However, our model is not intended to encompass the corona but rather the regions below it. Okamoto & De Pontieu (2011) suggest values for the Alfvén speed of around 556 km s^{-1} at the extreme end of the range of spicule heights (15″, or around 10.9 Mm); using this value for the Alfvén speed in the upper layer, the corresponding density ρ_2 can be estimated at around 2.57×10^{-11} g cm^{-3}, again with a kilogauss-strength background magnetic field for the purposes of this model. Comparing the 556 km s^{-1} estimate and the 22 km s^{-1} estimate gives $\alpha \approx 25$. However, Okamoto & De Pontieu (2011) also suggest a higher Alfvén speed at the surface, with their equivalent Alfvén speed ratio given as 3.39. Informed by these sources, we will consider values for α on the order of around 10, or equivalently a density ratio of around $\rho_1/\rho_2 = 100$. These estimates may be rather imprecise due to the highly variable nature of the solar atmosphere, especially in the vicinity of relatively small and dynamic features like spicules, hence the need to consider a range of values for these parameters. This range should give results that are compatible

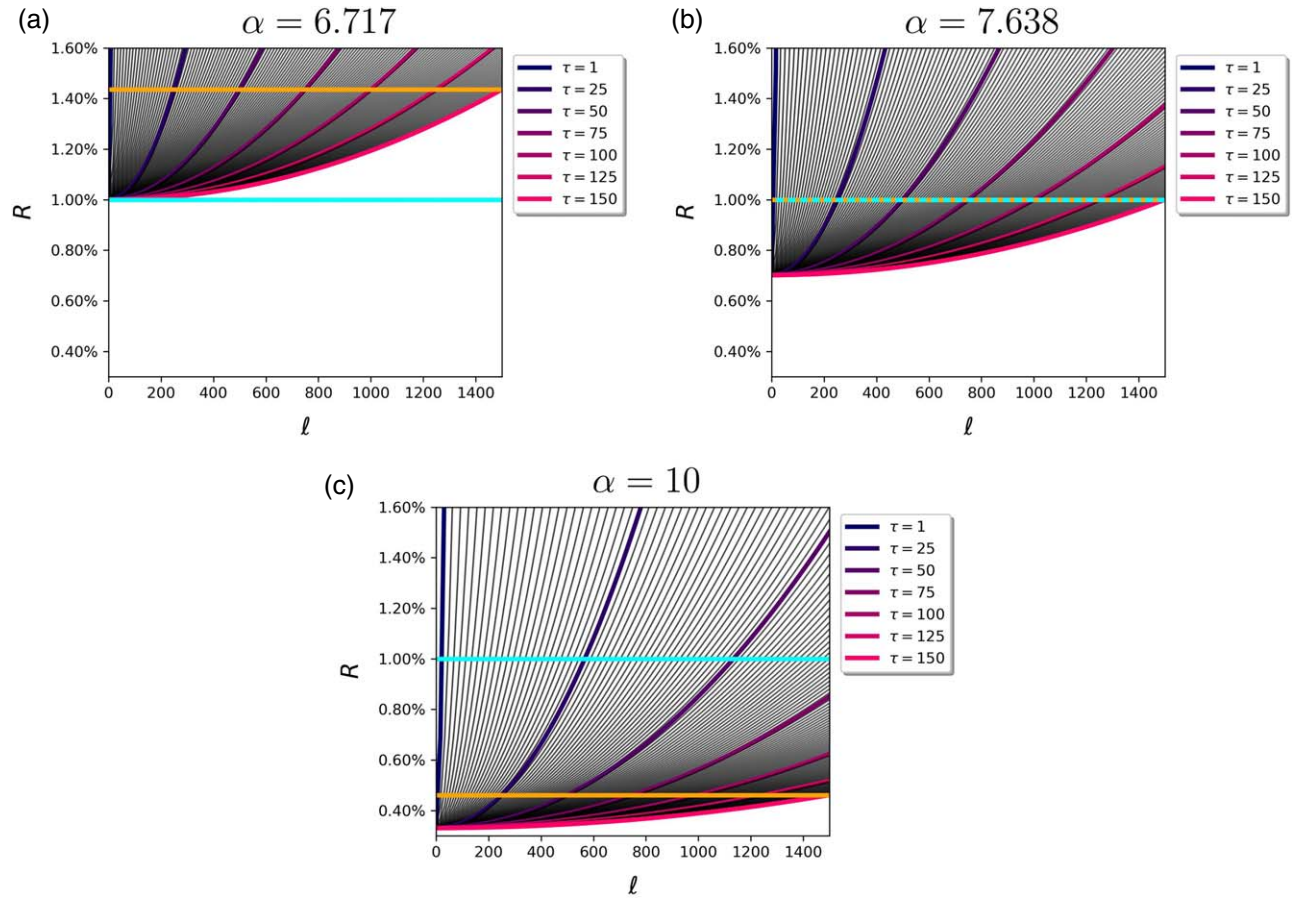

Figure 3. Plots of the mass–flux ratio R against the thickness of the transitional layer ℓ, illustrating the effect of varying pulse duration. Each curve represents a pulse with a different discrete value of the pulse duration τ between $\tau_{\min} = 1$s and $\tau_{\max} = 150$ s, all with constant $v_{A1} = 10$ km s^{-1}. Here, ℓ is only shown between 0 and the maximum length of any of the pulses within the chosen range, i.e., $v_{A1}\tau_{\max} = 1500$ km. According to our assumption of a thin transitional layer, the range of ℓ encompassed by the model is represented below and to the left of where the orange line intersects with each curve, at distinct values of $v_{A1}\tau$. The cyan line represents the 1% transmission threshold $R = 0.01$. We consider different values of α: (a) $\alpha = 6.717$, (b) $\alpha = 7.638$, and (c) $\alpha = 10$.

with the estimated ratio of the mass flux of the solar wind versus that of spicules (1%).

The ratio R strictly increases proportional to ℓ^2. This suggests that a wider transitional layer, in this case a more gentle gradient between the lower and upper regions in the model, results in stronger transmission of the wave. It should be noted that, if we take the limit as $\ell \to 0$, then the ratio depends only on α. Hence, this limit—equivalent to the case of the density discontinuity—gives the minimum value of the ratio for any particular value of α. This minimum ratio coincides with the result of Scalisi et al. (2021b); in particular, we find the minimum ratio matches the 1% estimate at $\alpha \approx 6.717$, just as in the example given in our previous paper. In fact, for $\alpha < 6.717$, the 1% threshold is exceeded for all ℓ. For $\alpha > 7.638$, the threshold is not reached for $0 < \ell < v_{A1}\tau$. The minimum value of the ratio is on the order of α^{-3} and so tends toward zero as $\alpha \to \infty$. Increasing the value of α not only reduces this minimum value but also means that the ratio increases more slowly as ℓ increases, as illustrated in Figure 2. Hence, we find that less of the mass would be transmitted above an arbitrarily thin transitional layer with a higher value of α, and also that increasing the width of the transitional layer has less effect with a higher value of α than it would with a lower value. This is, again, because the gradient in the transitional layer is more severe if there is a greater difference between the plasma density in the lower and upper regions.

It is worth noting that we also assumed earlier in our calculations (see Section 2.2.2) that the transitional layer was thin compared to the length of the pulse. An effect of this stipulation is that the travel time for the pulse to cross the transitional layer is negligible. As a result, we should focus on the results for the range $\ell < v_{A1}\tau$ in order to avoid loss of accuracy of the model. We are able to specify how the pulse is driven via the boundary conditions; in Scalisi et al. (2021a), we suggested that a pulse driven for around 150 s could reach a maximum vertical extent matching the height of spicules, and this is within the range of the average period of torsional Alfvén waves in MBPs (where our hypothetical wave driver is located) given by Jess et al. (2023). So, for example, if $\tau = 150$ s, along with an estimate of $v_{A1} = 10$ km s^{-1}, we could consider $\ell < 1500$ km. However, this may not be considered "thin" in comparison to the height of the chromosphere, so we may want to consider shorter pulses. These pulses would still propagate at the Alfvén speed, reaching the height of observed spicules within a few minutes, but would themselves be shorter in length than spicules. It is unclear whether the pulse needs to be driven continuously during the spicule's "rising" phase. If the driver is, for example, related to a photospheric or chromospheric swirl (Liu et al. 2019a, 2019b), then it is likely that the duration would be shorter than the lifespan of a spicule, because these features are observed to have average lifetimes of under 30 s—although this is only slightly less than the lifespan

of certain kinds of jets such as Type II spicules or RBEs (Kuridze et al. 2015). Again, it is useful to consider a range of possible values.

For a particular value of α, if the pulse duration τ is reduced then the mass–flux ratio increases faster as ℓ increases, i.e., a thinner transitional layer is required to reach the same ratio of transmitted mass. Regardless of the pulse duration, we find the same value of the ratio for a given α is always reached at $\ell = v_{A1}\tau$, the upper limit of the range of ℓ that we consider valid for this model. This maximum value of the ratio varies with α in a similar way to the minimum value (at $\ell = 0$), i.e., on the order of α^{-3}, and it reaches 1% at $\alpha \approx 7.638$.

The effect of varying τ is illustrated in Figure 3, for three discrete values of α representing different cases. In case (a), for $\alpha = 6.717$, the 1% transmission threshold (cyan line) is met at $\ell = 0$ regardless of the pulse duration, and at $\ell = v_{A1}\tau$ (orange line), the ratio is always just under 1.5%. In case (b), for $\alpha = 7.638$, the 1% threshold is always met at $\ell = v_{A1}\tau$ regardless of the pulse duration (cyan and orange lines are superimposed at the same value of $R = 0.01$). In case (c), we consider $\alpha > 7.638$, taking $\alpha = 10$ as an example; here, the ratio at $\ell = v_{A1}\tau$ is less than 0.5% regardless of the pulse duration, hence the mass flux present above the transitional layer in the higher solar atmosphere would be even less than 1% of the initial flux (for all values of $\ell < v_{A1}\tau$ satisfying our assumptions). This is acceptable in a physical context, because the 1% threshold refers to the total mass flux of spicules versus that of the solar wind, and spicules are of course not the only potential source of the solar wind. Therefore, 1% could be considered as the upper limit for the proportion of spicule material that may contribute to the solar wind. It follows that (c) is likely to be the most realistic of the three given cases. This is in line with the estimated values of the Alfvén speeds discussed earlier in this section.

There are some caveats concerning the physical interpretation of the results. First, although the model is not intended to include the corona, in reality the transitional layer does not end at a region of constant plasma density and the Alfvén speed may continue to increase with height above the photosphere. Therefore, it is likely that even less mass flux from the perturbations we describe will be present higher up in the atmosphere, and in the solar wind. However, it is true that the greatest change in density by far in the solar atmosphere occurs over a small length scale in the transition region, such that the corona can be modeled with constant Alfvén speed for the purposes of this work. Second, it is difficult to predict with this model what will happen to the plasma that has already been lifted. It is possible that a spicule's later trajectory would be influenced by both gravity and the effect of waves being repeatedly reflected, because many jets' trajectories are not purely ballistic (De Pontieu et al. 2007; Loboda & Bogachev 2017) and the plasma is likely to be affected by the waves in a different way at the top of the spicule compared to the at the base (Okamoto & De Pontieu 2011). Hence, the inclusion of gravity would be a useful addition to the model. Finally, the analysis presented here does not explicitly consider the variation of the background magnetic field with height, although—because the magnetic field strength is proportional to the Alfvén speed—it is taken into account by the current model and the effect of this variation can be inferred. However, tube expansion higher in the atmosphere will occur with the decreasing magnetic field strength inside the flux tube and may affect our estimates. A more thorough analysis of this effect could be the subject of a future study, building on the framework of the model presented here.

4. Conclusion

The model presented here is a useful diagnostic tool for investigating the compatibility of our ideas, allowing us to explore the processes occurring in the lower solar atmosphere, and providing some insight into the scale of the influence that spicules can have on the solar atmosphere beyond the chromosphere. We used our model to investigate whether mass flux would still be generated in the solar atmosphere above a transitional layer, due to a transmitted Alfvén wave. The results suggest that there would be flux present in that region on the order of 1% of the flux due to the initial pulse, and that in comparison to the case of a discontinuity, there is a slight increase.

In addition, the model suggests several things about spicules. Primarily, we suggest that the generation of jet-like motion can be driven or influenced by magnetic perturbations in the form of torsional Alfvén waves originating in strongly magnetic photospheric regions. We also find that these waves are restricted in the extent that they are able to propagate out into the atmosphere, putting a limit on the maximum height to which jets may be driven by them and suggesting that almost all of the mass lifted by this process will remain in the lower solar atmosphere rather than being ejected into the corona, as expected. However, despite that limit, some material from the jets may be carried higher into the atmosphere by the transmitted portion of the waves that were present during the formation of the jets, although only a small amount may eventually contribute to the solar wind.

R.E. is grateful to the Science and Technology Facilities Council (STFC, grant No. ST/M000826/1) U.K., the Royal Society (U.K.), and NKFIH (OTKA, grant No. K142987) Hungary for enabling this research. M.S.R. thanks the RSF for support via grant No. 20-12-00268.

ORCID iDs

Joseph Scalisi https://orcid.org/0000-0001-7070-6322
Michael S. Ruderman https://orcid.org/0000-0003-2324-8466
Robertus Erdélyi https://orcid.org/0000-0003-3439-4127

References

Abramowitz, M., & Stegun, I. A. 1965, Handbook of Mathematical Functions (New York: Dover)
Cranmer, S. R., & van Ballegooijen, A. A. 2005, ApJS, 156, 265
De Pontieu, B., Carlsson, M., Rouppe van der Voort, L. H. M., et al. 2012, ApJL, 752, L12
De Pontieu, B., McIntosh, S., Hansteen, V. H., et al. 2007, PASJ, 59, S655
De Wijn, A., Stenflo, J., & Tsuneta, S. 2009, SSRv, 144, 275
Ferraro, C. A., & Plumpton, C. 1958, ApJ, 127, 459
Jess, D. B., Jafarzadeh, S., Keys, P. H., et al. 2023, LRSP, 20, 1
Jess, D. B., Mathioudakis, M., Erdélyi, R., et al. 2009, Sci, 323, 1582
Jess, D. B., Pascoe, D. J., Christian, D. J., et al. 2012, ApJL, 744, L5
Keys, P. H., Mathioudakis, M., Jess, D. B., et al. 2013, MNRAS, 428, 3220
Kuridze, D., Henriques, V., Mathioudakis, M., et al. 2015, ApJ, 802, 26
Liu, J., Carlsson, M., Nelson, C. J., & Erdélyi, R. 2019a, A&A, 632, A97
Liu, J., Nelson, C. J., Snow, B., Wang, Y., & Erdélyi, R. 2019b, NatCo, 10, 3504
Loboda, I. P., & Bogachev, S. A. 2017, A&A, 597, A78
Makita, M. 2003, PNAOJ, 7, 1

Okamoto, T. J., & De Pontieu, B. 2011, ApJL, 736, L24
Priest, E. 2014, Magnetohydrodynamics of the Sun (Cambridge: Cambridge Univ. Press)
Roberts, B. 2019, MHD Waves in the Solar Atmosphere (Cambridge: Cambridge Univ. Press)
Scalisi, J., Oxley, W., Ruderman, M. S., & Erdélyi, R. 2021a, ApJ, 911, 39
Scalisi, J., Ruderman, M. S., & Erdélyi, R. 2021b, ApJ, 922, 118
Sterling, A. C. 2000, SoPh, 196, 79
Tomczyk, S., McIntosh, S. W., Keil, S. L., et al. 2007, Sci, 317, 1192
Tsiropoula, G., Tziotziou, K., Kontogiannis, I., et al. 2012, SSRv, 169, 181
van Ballegooijen, A. A., Asgari-Targhi, M., Cranmer, S. R., & DeLuca, E. E. 2011, ApJ, 736, 3
Vernazza, J. E., Avrett, E. H., & Loeser, R. 1973, ApJ, 184, 605
Vernazza, J. E., Avrett, E. H., & Loeser, R. 1981, ApJS, 45, 635